A PET Prototype for "In-Beam" Monitoring of Proton Therapy

Sara Vecchio, *Student Member, IEEE*, Francesca Attanasi, Nicola Belcari, Manuela Camarda, G. A. Pablo Cirrone, Giacomo Cuttone, Francesco Di Rosa, Nico Lanconelli, Sascha Moehrs, *Student Member, IEEE*, Valeria Rosso, Giorgio Russo, and Alberto Del Guerra, *Senior Member, IEEE*

***Abstract*—The in-beam PET is a novel PET application to image the β^+ activity induced in biological tissues by hadronic therapeutic beams. Thanks to the correlation existing between beam-delivered dose profiles and beam-induced activity profiles, in vivo information about the effective ion paths can be extracted from the in-beam PET image. In-situ measurements, immediately after patient irradiation, are recommended in order to exploit the maximum statistics, by also detecting the contribution provided by the very short lived isotopes, e.g. ^{15}O. A compact, dedicated tomograph should then be developed for such an application, so as to be used in the treatment room.**

We developed a small PET prototype in order to demonstrate the feasibility of such a technique for the monitoring of proton therapy of ocular tumors at the CATANA facility (Catania, Italy). The prototype consists of two planar heads with an active area of about 5 cm $\times$ 5 cm. Each head is made up of a square position sensitive photomultiplier (Hamamatsu H8500) coupled to a matrix of the same size of LYSO scintillating crystals (2 mm $\times$ 2 mm $\times$ 18 mm pixel dimensions). Dedicated, compact electronic boards are used for the signal multiplexing, amplification and digitization. The distance between the pair can be varied from 10 cm up to a maximum of about 20 cm.

The validation of the prototype was performed on plastic phantoms using 62 MeV protons at the CATANA beam line. Different dose distributions were delivered and a good correlation between the distal fall-off of the activity profiles and of the dose profiles was found, i.e., better than 2 mm along the beam direction.

***Index Terms*—Eye therapy, in-beam monitoring, PET, proton.**

I. Introduction

ALL particles used in hadrontherapy, protons included, induce nuclear reactions in the biologic material which lead to the production of β^+ emitters, i.e., mainly ^{15}O and ^{11}C from their corresponding stable isotopes [1], [2]. By using ions like carbon, oxygen or fluorine, there is a further production of other β^+ emitters through the fragmentation of beam ions themselves. The induced activity can be measured with the so-called "in-beam PET" to extract in-vivo information about the effective ion path and stopping point. By comparison with the calculated activity distribution, as evaluated from the dose profile of the treatment plan, an indication of discrepancies from the planned dose can be extracted. Different processes underlie β^+-activation and the dominant mechanism of energy deposition: they are nuclear and atomic processes, respectively. The difference of the physical processes causes a significant difference between the activity and the dose distributions produced by the same beam. In particular, with proton beams the 5–20 MeV threshold for nuclear reactions in target tissue produces an activity distribution that ends a few millimeters before the Bragg peak [3]. However, the distal dose fall-off is expected to be correlated with the activity distal edges, since both are produced by the interaction of protons with matter.

The determination of the correlation between the range of incident particles and the induced activity distribution for the specific ion beam is a fundamental step of the "in-beam" PET technique. In fact, the knowledge of such correlation allows the proper inference of the spatial distribution of the delivered dose from the PET-image. One possible approach, adopted in the case of proton irradiation of homogeneous materials, is the use of a filter function [4], which must be determined starting from the beam energy distribution, the beam isotope, and the PET detector characteristics. By the convolution of the activity distribution with the filter, it will be possible to unfold the dose information carried by the measured PET image and to compare the delivered dose distribution with the planned one. Any significant disagreement is an indication of variations in the delivery process, that could be accounted for and possibly corrected for before the following fraction of therapy.

Post irradiation ("off-beam") usage of commercial full-ring PET or PET/CT scanners has been experimented [5], [6].

For the dose profile monitoring, the possibility of on-line measurements, i.e., immediately after patient irradiation, is of great importance, since one collects the maximum statistics by detecting the activity contribution also provided by the very short lived isotopes (e.g., ^{15}O, which has a 2 min half life). Moreover, in-beam measurements avoid alignment errors that could arise when moving the patient from the therapy to the PET location, and diminish the biological wash out of the produced isotopes, that would happen during the transfer time.

The positive clinical impact of in-beam PET has been already demonstrated at GSI (Darmstadt) for ^{12}C irradiation by using

Manuscript received March 03, 2008; revised August 05, 2008 and October 06, 2008. Current version published February 11, 2009. This work was supported in part by the INFN and by the MIUR in the framework of the PRIN2006 program, number 2006025517_003.

S. Vecchio, F. Attanasi, N. Belcari, M. Camarda, S. Moehrs, V. Rosso, and A. Del Guerra are with the Department of Physics, University of Pisa, I-56127 Pisa, Italy, and also with INFN-Pisa, I-56127 Pisa, Italy (e-mail: sara.vecchio@pi.infn.it; francesca.attanasi@pi.infn.it; belcari@df.unipi.it; manuela. camarda@pi.infn.it; sascha.moehrs@df.unipi.it; valeria.rosso@pi.infn.it; alberto. delguerra@df.unipi.it).

G. A. Pablo Cirrone, G. Cuttone, F. Di Rosa, and G. Russo are with INFN-LNS, I-95123 Catania, Italy (e-mail: cirrone@lns.infn.it; cuttone@lns.infn.it; dirosa@lns.infn.it; giorgiorusso@lns.infn.it).

N. Lanconelli is with the Department of Physics, University of Bologna, I-40127 Bologna, Italy, and also with INFN-Bologna, I-40127 Bologna, Italy (e-mail: lanconelli@bo.infn.it).

Digital Object Identifier 10.1109/TNS.2008.2008306

a commercial PET scanner adapted to the purpose. The GSI group is the first one to use such monitoring technique in clinical routine [7]. Stimulated by this successful experience and by the growing number of ion beam therapy facilities worldwide, the employment of PET imaging for quality assurance has been investigated also for protons [8]–[10], $^{3}\mathrm{He}$ [11], $^{16}\mathrm{O}$ [12] and even photons [13]. Besides the in-beam PET tomograph at GSI, only few more systems have been recently installed in Japan [14], [15] and Italy [16].

The CATANA center (Centro di AdroTerapia e Applicazioni Nucleari Avanzate [17]) has developed a proton therapy facility for the treatment of ocular lesions with a 62 MeV proton beam from a Superconducting Cyclotron at INFN-LNS (Istituto Nazionale di Fisica Nucleare—Laboratori Nazionali del Sud) in Catania.

The DoPET project (Dosimetry with a Positron Emission Tomograph) aims to realize a PET system dedicated to "in-beam" proton-therapy monitoring. The system has been validated through a series of measurements on polymethylmethacrylate (PMMA, $\mathrm{C_5H_8O_2}$) phantoms. The irradiation setup has been chosen according to clinical conditions applied in tumour treatment monitoring at CATANA. The obtained results are presented in the following sections.

II. Experimental Apparatus

The prototype tomograph consists of two planar heads, with an active area of about 5 cm $\times$ 5 cm (see Fig. 1). Each head is made up of a square position sensitive photomultiplier (Hamamatsu H8500 [18]) coupled to a matrix of LYSO ($\mathrm{Lu_{2(1-x)}Y_{2x}SiO_5}$, $x \approx 0.1$) scintillating crystals (21 $\times$ 21 pixel matrix, with 2 mm $\times$ 2 mm $\times$ 18 mm pixel dimensions) from Hilger Crystals Ltd (UK).

A multiplexed read-out [19] is chosen to reduce the number of acquired signals from the 64 anodes to only 4 signals per head. Dedicated, compact electronic boards are used for the signal amplification and digitization. Coincidences rates above 50 kHz roughly correspond to dead time loss higher than 10% and more than 25% of pile-up loss. However, this is not a problem for this application, since typical coincidence rates during "in-beam" measurements are on the order of 1 kHz or below.

The detector calibration procedure includes gain compensation, sensitivity normalization, dead time corrections and subtraction of coincidence background from random occurrences as well as from the scintillator natural radioactivity (the radioisotope $^{176}\mathrm{Lu}$ is present in the natural Lu composition). The radionuclide decay corrections are performed automatically only during calibration measurements, i.e., when the acquired radioactive source is made up of a single radionuclide species. No preliminary decay correction was applied in the case of data acquisition of proton-induced activity, but a time analysis of acquired data decay can be performed to deconvolve $^{15}\mathrm{O}$ and $^{11}\mathrm{C}$ contributions to the measured activity.

The SimSET [20] package has been adopted to model the physical processes and the detector, for the optimization of detector design and acquisition protocols.

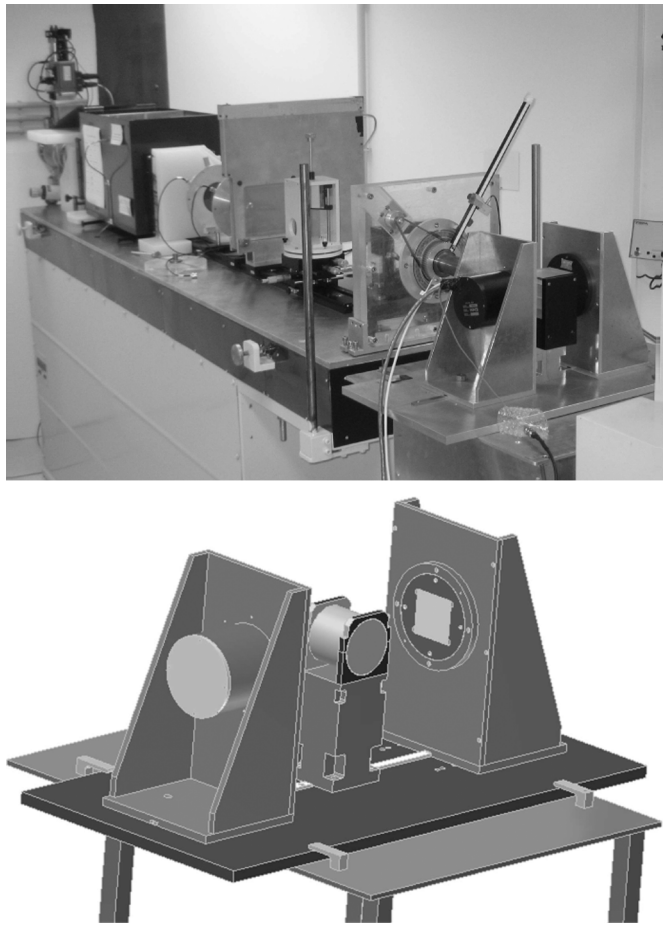

Fig. 1. Schematic view of the prototype: the two detector heads and the plastic phantom are held by an aluminum-alloy support. The entire instrument is then placed on a plane which is aligned with respect to the beam direction. Protons impinge on one base of the cylindrical phantom.

The distance between the two heads can be varied from 10 cm up to a maximum of about 20 cm. In the presented measurements, the detector heads were symmetrically placed 14 cm apart with respect to the measured activity region.

The overall detection efficiency measured with a $^{22}\mathrm{Na}$ point source (150 kBq) at the center of the field of view (FoV) was found to be 1.0% in the energy window [150, 850] keV and 0.7% in the energy window [350, 850] keV. The first energy window rejects electronics noise and is used to profit from the maximum statistics, while the latter one allows the rejection of phantom scattering and background from natural $^{176}\mathrm{Lu}$ radioactivity. The measure of detection efficiency does not presently include any scattering correction.

III. Reconstruction Algorithm

Dealing with low statistics, it is essential to use effectively the limited data set. We have utilized a 3D Maximum Likelihood Expectation Maximization (3D ML-EM) reconstruction that makes use of all the collected lines-of-response. A multi-ray method [21] is utilized for the calculation of the probability matrix, taking into account the geometry as well as the physics of photon detection.

The limited angular acceptance of the prototype makes it impossible to achieve an exact reconstruction of the activity distribution in all three dimensions. However, for proton therapy monitoring, a very important goal is to obtain a resolution on the order of the millimeter along the beam direction.

The spatial resolution has been measured on the ML-EM reconstructed image with a $^{22}\mathrm{Na}$ point source (1 mm diameter) placed in the center of the FoV. It is 1.7 mm (FWHM) in the plane parallel to the heads (see Fig. 1). The same result (within 0.1 mm) has been obtained with the source in air or embedded in PMMA, reconstructing data with 1 mm and 0.5 mm voxel sizes, and using energy selection [150, 850] keV, as well as [350, 850] keV.

IV. Unfolding Procedure

The calculation of the filter function to unfold the dose distribution requires the a priori knowledge of both the delivered dose and the induced activity for some reference beams with a known energy distribution. For the dose and activity calculation of proton beams, we currently adopt a semi-analytic algorithm. The dose calculation is separated into two independent steps: the evaluation of the (angular, spatial and energy) distributions of proton beams as determined by the specific accelerator line and the physical interactions of the beam in the patient. The first one is obtained from a GEANT4 simulation [22]. The in-depth evolution of the proton energy distribution is then obtained through the numerical integration of a Fokker-Planck equation [23].

The chosen reference beams are monoenergetic proton beams. Dose profiles and the induced activity profiles (mainly from $^{11}\mathrm{C}$ and $^{15}\mathrm{O}$) along the beam depth x are well approximated by a linear combination of a family of analytical functions $\{\tilde{Q}\}$ [4], defined as

$$\tilde{Q}_\nu(x) = G(x) * P_\nu(x), \tag{1}$$

where

$$G(x) = \frac{1}{\sqrt{2\pi}} \exp -\frac{x^2}{2},$$
$$P_\nu(x) = \begin{cases} \frac{1}{\Gamma(\nu)} x^{\nu-1}, & \text{if } x \geq 0, \\ 0, & \text{otherwise.} \end{cases} \tag{2}$$

in which ν is a real number and $\Gamma(\nu)$ is the extension of the factorial (!) to real number arguments and is used for normalization purposes. The convolution of two arbitrary $\tilde{Q}$-functions can be algebraically evaluated from the analytic expression of the starting functions. Therefore the convolution filter from dose to each activity profile is easily extrapolated. The linear combination of each isotope filter would produce the proper filter for deriving activity distributions from dose distributions. Each weight coefficient of the linear combination represents the fraction of activity assigned to the given isotope for the specific measurement.

The first validation of this analytical approach to the analysis of dose-activity correlation has been already presented in [23]. From the study it emerges the applicability of this approach as an alternative to full-blown Monte Carlo simulation for dose verification. The agreement between filtered-dose and measured-activity in the low energy range ([40, 70] MeV) is consistent with the existence of one universal filter function to convert dose into activity profile, regardless of the beam energy. This result supports the efforts to invert the filter itself so as to achieve the proper dosimetric goal.

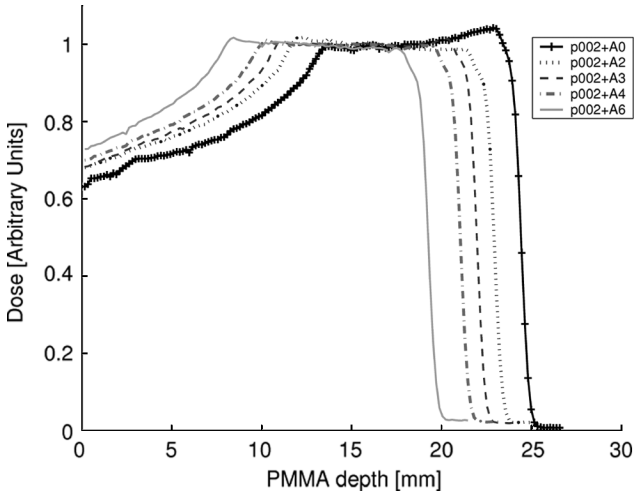

Fig. 2. In-depth dose profiles of beam line configurations used at CATANA for range shift measurements. Curves are normalized to the middle point of the modulation plateau. Eye-tissue equivalent thicknesses are: $\mathrm{A0} = 0$ mm, $\mathrm{A2} = 2$ mm, $\mathrm{A3} = 3$ mm, $\mathrm{A4} = 4$ mm, $\mathrm{A6} = 6$ mm. Thicknesses in PMMA of range shifters are reported in the text.

V. Measurement Setup

The feasibility of range monitoring was studied in monoenergetic and energy modulated proton beams. Homogeneous PMMA phantoms were irradiated at the INFN-LNS cyclotron, using the beam line of the CATANA facility. The proton beam available at CATANA is a monoenergetic 62 MeV proton beam, which is passively shaped to different energy distributions. Range shifters of different PMMA thicknesses are inserted along the beam path to obtain lower proton beam energies, while energy modulated proton beams are produced using modulating wheels. A 25 mm diameter brass collimator has been adopted as final collimator for all the phantom irradiations. 30 Gy irradiations were usually employed for quantitative measurements. However, measurements at clinical conditions of one therapy fraction (15 GyE) delivery were also tested. Before each run, routine dosimetry protocol is followed to control the dose delivery. The absolute measurements are performed in water with a plane parallel Markus ion chamber, as required by the IAEA TRS-398 protocol [24], and following the procedure described in [17]. For the relative dose measurement a Si diode (CCO diode BPW34) is chosen [25]. The dose profiles measured with the silicon diode were used to predict the activity distribution applying the algorithm described in [23].

In Figs. 2 and 3 the in-depth dose profiles of beam configurations used to irradiate PMMA phantoms for DoPET acquisitions are shown. Range shifters and modulation wheels used were selected from those employed by the CATANA group for proton-therapy. Profiles in Fig. 2 are obtained with a modulation of 10.8 mm in PMMA (labeled as p002), and different range shifters. Eye-tissue equivalent thicknesses of the range shifters inserted are $\mathrm{A0} = 0$ mm, $\mathrm{A2} = 2$ mm, $\mathrm{A3} = 3$ mm, $\mathrm{A4} =$

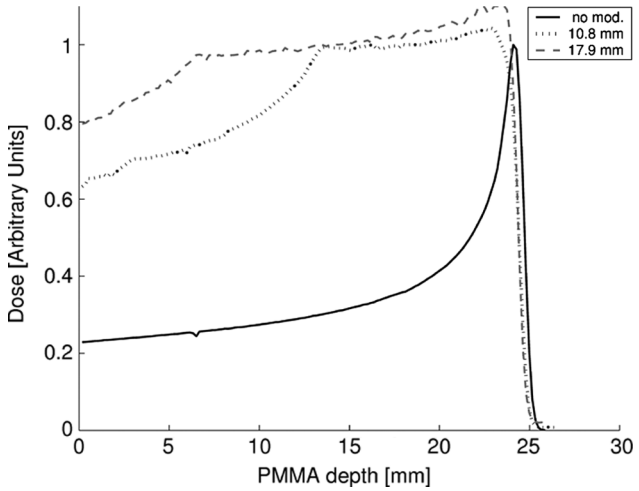

Fig. 3. In-depth dose profiles of beam line configurations used at CATANA for modulation width detection. Two modulation wheels and a full-energy beam were used, with no range shifter inserted. Spread-out curves are normalized to the middle point of the modulation plateau. The single Bragg peak is normalized to its maximum. Eye-tissue equivalent modulation widths are: 0 mm, 12 mm, 20 mm. Modulation widths in PMMA are reported in the legend and in the text.

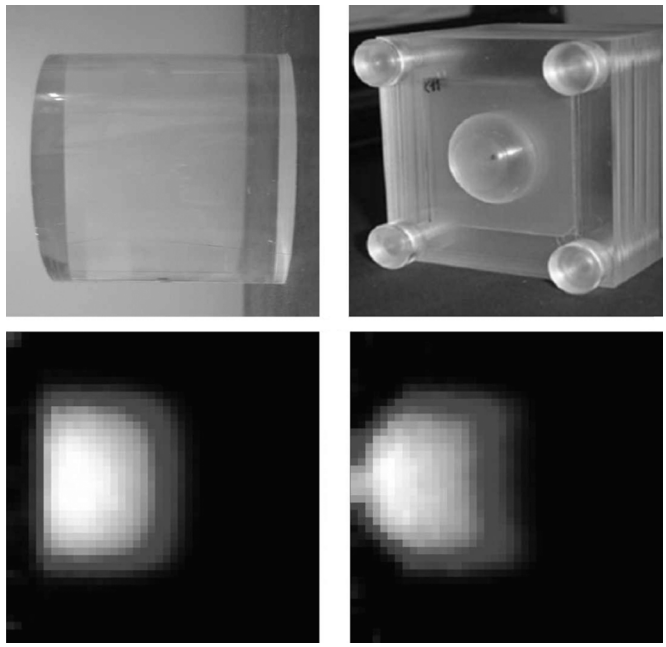

Fig. 4. Visual comparison between phantoms with different entrance surfaces. Left: flat entrance surface. Right: eye-shaped entrance surface. Top: photographs of the used PMMA phantoms. Bottom: central slice (42 × 42 voxels, 1.076 mm thick) of the reconstructed images, with proton impinging from the left. No rigid support was available for the eye-shaped phantom; therefore its displacement in the FoV could not reproduce that of the cylindrical phantom (about 5 mm difference along beam direction).

4 mm and $\mathrm{A6} = 6$ mm, which correspond to PMMA equivalent thicknesses of $\mathrm{A0} = 0$ mm, $\mathrm{A2} = 1.87$ mm, $\mathrm{A3} = 2.89$ mm, $\mathrm{A4} = 3.85$ mm, $\mathrm{A6} = 5.77$ mm, respectively.

Profiles in Fig. 3 are obtained with no range shifter and different modulation wheels. Modulation widths in eye-tissue are 12 mm and 20 mm, that correspond to PMMA modulation widths of 10.8 mm and 17.9 mm, respectively. A baseline configuration with no range shifter and no modulation wheel is also shown.

Phantoms were placed at the center of the FoV, and the distance between the heads was set to 14 cm. Clinical conditions for eye therapy would suggest an asymmetric configuration, or larger head-to-head distances (at least equal to the head diameter), which will be tested with a larger version of the DoPET detector that is now under construction. The phantom position along the beam direction was chosen so as to place the distal fall-off of activity distribution at the center of the FoV, where the spatial resolution and the detector efficiency are maximum.

The energy window of [350, 850] keV has been chosen for reconstructed data, in order to reject $^{176}\mathrm{Lu}$ background radioactivity in the crystal and scattering contribution in phantom. The reconstruction algorithm divides the FoV in $42 \times 42 \times 130$ voxels, but only the $42 \times 42 \times 42$ central volume is reconstructed; the 42 × 42 voxels central slice (1.076 mm thick) is used for the results presented in the next section.

VI. Results and Discussion

Three runs of measurements have been performed for the validation on cylindrical plastic phantoms. The preliminary results obtained during the first run have been already presented in [16]. The detection capability of 2 mm shifts in proton range was only qualitatively shown for proton irradiations in non-clinical configurations (sharp, unmodulated Bragg peaks and 40–60 Gy dose delivery). In this paper we report the first attempt of quantitative analysis of the results obtained in two successive runs. Modulated proton beams and calibrated dose delivery were used.

Fig. 4 shows the reconstructed images of phantom β^+ activation obtained using a modulation of 12 mm eye-tissue equivalent matter (10.8 mm in PMMA) and 2 mm eye-tissue equivalent range shifter ($\mathrm{A2} = 1.87$ mm in PMMA), i.e., a possible therapy configuration. One therapy dose fraction (15 GyE) has been delivered in about 1 minute as in clinical conditions. The PET acquisition has been done for the following 15 minutes. The results using the cylindrical phantom and an eye-shaped phantom [26] can be visually compared from the picture.

Since these first results appeared statistical-limited, all the other measurements performed were based on acquisitions performed after a higher dose delivery (30 Gy), corresponding to about twice the therapy dose fraction. For doses of 30 Gy in 1 minute over a PMMA volume of about 6 cm^3 (i.e., no range shifter in the beam line), the DoPET detector collected about 10^5 coincidences for a head-to-head distance of 14 cm and an acquisition time of 30 minutes after the end of the irradiation.

The time analysis of the acquired data assigns 75% of measured activity to $^{11}\mathrm{C}$, and about all the remaining 25% to $^{15}\mathrm{O}$. This confirms the effectiveness of the in-beam measurement to increase statistics with respect to off-beam acquisitions that cannot profit from the short-lived $^{15}\mathrm{O}$ activation.

Fig. 5 shows the central slices of the activity distributions reconstructed in two different runs (February 2007 and May 2007) with the same beam configurations, i.e., a modulation of 10.8 mm, and three different range shifters (A2 has been used in the second run only). The 50% level contour plot has been

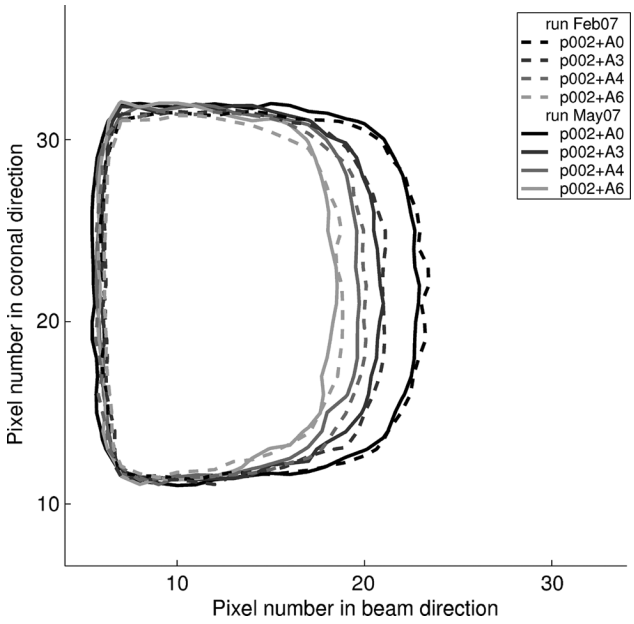

Fig. 5. 50% contour activity profiles of the central slice (42 × 42 voxels, 1.076 mm thick) of the reconstructed images for the activity acquired after 30 Gy irradiations using 10.8 mm modulation and different range shifters (see Fig. 2). Solid lines correspond to measurements performed on May 2007, whereas dashed lines correspond to February 2007 measurements. The same grey tone corresponds to the same beam line configuration. The proton beam impinges from left. The proximal edge of the cylindrical phantom is in the vertical line placed at pixel #3 along the beam direction. The center of the FoV is at point (21,21) in the plot.

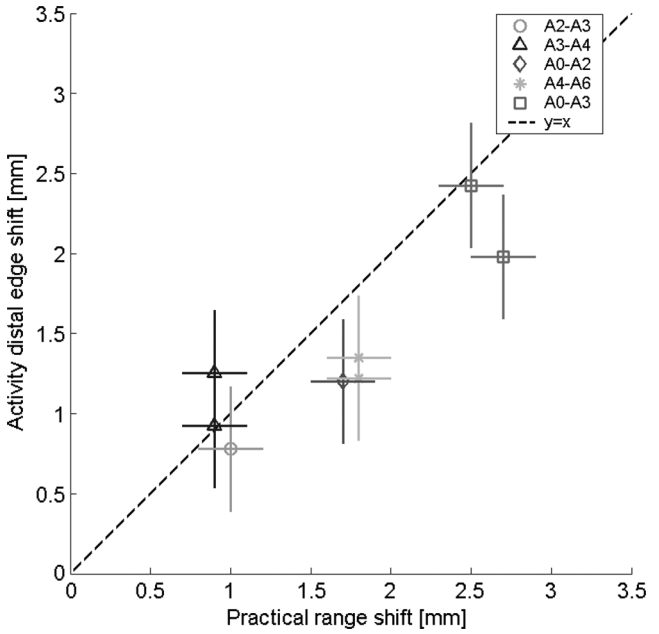

Fig. 6. Correlation between range shifts and activity distal edge shifts in PMMA phantoms. The legend explains the range shifter combinations used to measure the shifts. Uncertainties are 0.2 mm in practical range shift and 0.3 mm in activity distal edge shift. The expected linear correlation $y = x$ is shown by a dashed line.

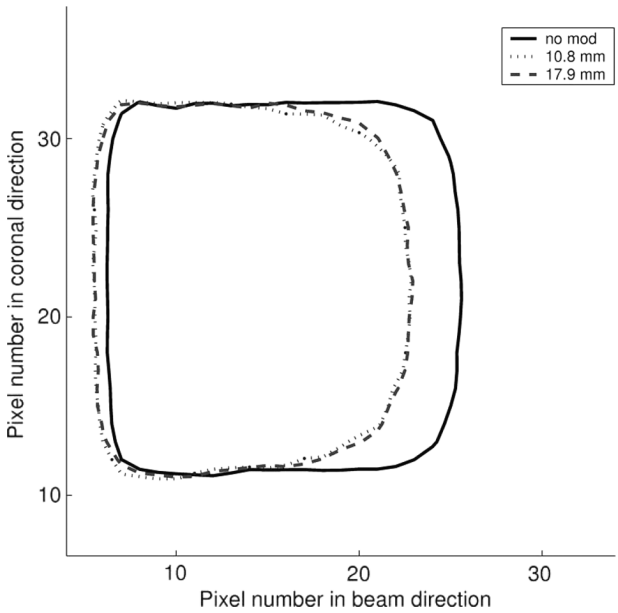

Fig. 7. 50% contour activity profiles of the central slice (42 × 42 voxels, 1.076 mm thick) of the reconstructed images for activity acquired after irradiations using different modulation widths (see Fig. 3). The proton beam impinges from left. The proximal edge of the cylindrical phantom is in the vertical line placed at pixel #3 in the beam direction. The center of the FoV is at point (21,21) in the plot.

chosen for visualization and analysis because it appeared to be less sensitive to the reconstruction algorithm and to image fluctuations. The comparison of the results from the two runs supports the reliability and reproducibility of our setup from run to run.

Since systematic errors in the alignment of the phantom have not yet been evaluated, an unknown offset could affect the inference of practical beam range from the position of the activity distal edge in these data. Thus we prefer to present our results as a correlation between activity shifts and range shifts.

Shifts in activity profiles were measured as shifts in the 50% distal fall-off of the activity profile along the beam direction in the central slice of the reconstructed images. Profiles are evaluated on a single voxel row. Integration on more pixel rows would lead to a reduced statistical fluctuation in the results along beam direction, but would make the results dependent on the activity distribution along the orthogonal directions. Shifts in proton range were measured as shifts in practical range measured from in-depth dose profiles (see dose configurations presented in Fig. 2).

The correlation between activity distal edge shifts and practical range shifts for all the measurements performed in the two runs is shown in Fig. 6. If the slope of the distal activity profile is assumed to be energy independent to a first order approximation [23], then the correlation between practical range and activity distal edge shifts should lay on the bisector axis $y = x$. The practical range is determined within roughly $\pm 100\ \mu$m, that is the uncertainty of the diode positioning system. Uncertainty on the measurements of the practical range shift, is then estimated to be 0.2 mm. Uncertainty on the measurements of the activity distal edge mainly depends on image fluctuation, and was evaluated as the standard deviation from the average result of repeated acquisitions. The resulted value is less than 0.2 mm, therefore the uncertainty on activity shifts is about 0.3 mm.

Fig. 7 shows the 50% contour activity profiles of the central slice of the reconstructed images obtained from acquisitions after irradiations using different beam modulations, and no range shifter, i.e., a dose configuration as presented in Fig. 3.

The difference in activity profiles between modulated and unmodulated irradiations is well detected, as a variation on both in-depth and coronal distributions. The phantom was in the same position for each measurement (i.e., the activity profiles start at pixel #3 in the beam direction). From Fig. 7 it appears that the full-energy beam proximal edge is less steep than those of modulated beams, since the 50% level is reached at a higher depth. No difference is visible between the 50% contour activity profiles of the two modulated irradiations. Alternative codings for detection of differences in activity distributions (using both linear profiles or multi-level contour plots) will be investigated before drawing a final conclusion. Results are consistent with the analytic prediction obtained in [23].

VII. Summary and Future Work

The "in-beam" performance of the DoPET prototype has been evaluated. The reproducibility of results has been verified.

Range shifts down to 1 mm have been detected. From detector symmetries, the capability of detecting 1 mm deviations from planned dose can be also assumed in the vertical direction.

A more accurate analysis must be done before performing clinical validation. In particular the sensitivity of the detector to energy modulation should be better understood and non-uniform phantoms should be used for a quantitative analysis in the vertical direction.

The positive results obtained by this first prototype support the construction of a (larger) clinical version of such a dedicated "in-beam" PET for hadrontherapy quality assurance. The development of this larger detector is ongoing.

References

[1] G. W. Bennett, J. O. Archambeau, B. E. Archambeau, J. I. Meltzer, and C. L. Wingate, "Visualization and transport of positron emission from proton activation in vivo," *Science*, vol. 200, pp. 1151–1153, 1978.

[2] A. Del Guerra, G. Di Domenico, M. Gambaccini, and M. Marziani, "A Monte Carlo simulation of the possible use of positron emission tomography in proton radiotherapy," *Nucl. Instr. Meth. A*, vol. 345, pp. 379–384, 1994.

[3] U. Oelfke, G. K. Y. Lam, and M. S. Atkins, "Proton dose monitoring with PET: Quantitative studies in Lucite," *Phys. Med. Biol.*, vol. 41, pp. 177–196, 1996.

[4] K. Parodi and T. Bortfeld, "A filtering approach based on Gaussian-powerlaw convolutions for local PET verification of proton radiotherapy," *Phys. Med. Biol.*, vol. 51, pp. 1991–2009, 2006.

[5] Y. Hishikawa, K. Kagawa, M. Murakami, H. Sakai, T. Akagi, and M. Abe, "Usefulness of positron-emission tomographic images after proton therapy," *Int. J. Radiation Oncology Biol. Phys.*, vol. 53, pp. 1388–1391, 2002.

[6] K. Parodi, H. Paganetti, E. A. Shih, S. Michaud, J. S. Loeffler, and T. F. Delaney *et al.*, "Patient study on in-vivo verification of beam delivery and range using PET/CT imaging after proton therapy," *Int. J. Radiat. Oncol. Biol. Phys.*, vol. 68, pp. 920–934, 2007.

[7] W. Enghardt, P. Crespo, F. Fiedler, R. Hinz, K. Parodi, J. Pawelke, and F. Pönisch, "Charged hadron tumour therapy monitoring by means of PET," *Nucl. Instr. Meth. A*, vol. 525, pp. 284–288, 2004.

[8] D. W. Litzenberg, D. A. Roberts, M. Y. Lee, K. Pham, A. M. Vander Molen, R. Ronningen, and F. D. Becchetti, "On-line monitoring of radiotherapy beams: Experimental results with proton beams," *Med. Phys.*, vol. 26, pp. 992–1006, 1999.

[9] K. Parodi, W. Enghardt, and T. Haberer, "In-beam PET measurements of radioactivity induced by proton beams," *Phys. Med. Biol.*, vol. 47, pp. 21–36, 2002.

[10] T. Inaniwa, T. Tomitani, T. Kohno, and T. Kanai, "Quantitative comparison of suitability of various beams for range monitoring with induced activity in hadron therapy," *Phys. Med. Biol.*, vol. 50, pp. 1131–1145, 2005.

[11] F. Fiedler, P. Crespo, M. Sellesk, K. Parodi, and W. Enghardt, "The feasibility of in-beam PET for therapeutic beams of $^{3}\mathrm{He}$," *IEEE Trans. Nucl. Sci.*, vol. 53, no. 4, pp. 2252–2259, Aug. 2006.

[12] T. Inaniwa, T. Kohno, T. Tomitani, and S. Sato, "Monitoring the irradiation field of $^{12}\mathrm{C}$ and $^{16}\mathrm{O}$ SOBP beams using positron emitters produced through projectile fragmentation reactions," *Phys. Med. Biol.*, vol. 53, pp. 529–542, 2008.

[13] D. Möckel, H. Müller, J. Pawelke, M. Sommer, E. Will, and W. Enghardt, "Quantification of β^{+} activity generated by hard photons by means of PET," *Phys. Med. Biol.*, vol. 52, pp. 2515–2530, 2007.

[14] Y. Iseki, H. Mizuno, Y. Futami, T. Tomitani, T. Kanai, M. Kanazawa, A. Kitagawa, T. Murakami, T. Nishio, M. Suda, E. Urakabe, A. Yunoki, and H. Sakai, "Positron camera for range verification of heavy-ion radiotherapy," *Nucl. Instrum. Methods A*, vol. 515, pp. 840–849, 2003.

[15] T. Nishio, T. Ogino, K. Nomura, and H. Uchida, "Dose-volume delivery guided proton therapy using beam on-line PET system," *Med. Phys.*, vol. 33, p. 41907, 2006.

[16] F. Attanasi, N. Belcari, M. Camarda, G. A. P. Cirrone, G. Cuttone, A. Del Guerra, F. Di Rosa, N. Lanconelli, V. Rosso, G. Russo, and S. Vecchio, "Preliminary results of an in-beam PET prototype for proton therapy," *Nucl. Instr. Meth. A*, vol. 591, pp. 296–299, 2008.

[17] G. A. P. Cirrone, G. Cuttone, P. A. Lojacono, S. Lo Nigro, V. Mongelli, I. V. Patti, , G. Privitera, L. Raffaele, D. Rifuggiato, M.G. Sabini, V. Salamone, C. Spatola, and L.M. Valastro, "A 62-MeV proton beam for the treatment of ocular melanoma at Laboratori Nazionali del Sud-INFN," *IEEE Trans. Nucl. Sci.*, vol. 51, no. 5, pp. 860–864, Oct. 2004.

[18] Hamamatsu Technical Information, Japan, "H8500 PSPMT," 2003.

[19] N. Belcari, A. Del Guerra, M. Camarda, L. Spontoni, S. Vecchio, and D. Bianchi, "Performance of a four-output front-end electronics for multi-anode PMTS readout of scintillator arrays," *Nucl. Instr. Meth. A*, vol. 572, pp. 335–337, 2007.

[20] SimSET, Univ. Washington, Div. Nucl. Med., Seattle, WA, "SimSET homepage," 2006. [Online]. Available: http://depts.washington.edu/simset/html/simset_main.html

[21] S. Moehrs, M. Defrise, N. Belcari, A. Del Guerra, A. Bartoli, S. Fabbri, and G. Zanetti, "Multi-ray based system matrix generation for 3D PET reconstruction," *Phys. Med. Biol.*, vol. 53, no. 23, pp. 6925–6945, 2008.

[22] G. A. P. Cirrone, G. Cuttone, F. Di Rosa, L. Raffaele, G. Russo, S. Guatelli, and M. G. Pia, "The GEANT4 toolkit capability in the hadron therapy field: Simulation of a transport beam line," *Nucl. Phys. B—Proc. Suppl.*, vol. 150, pp. 54–57, 2006.

[23] F. Attanasi, N. Belcari, M. Camarda, A. Del Guerra, S. Moehrs, V. Rosso, S. Vecchio, N. Lanconelli, G. A. P. Cirrone, F. Di Rosa, and G. Russo, "Experimental validation of the filtering approach for dose monitoring in proton therapy at low energy," *Physica Medica—EJMP*, vol. XXIV, pp. 102–106, 2008.

[24] P. Andreo, D. T. Burns, K. Hohlfeld, M. Saiful Huq, T. Kanai, F. Laitano, W. Smyth, and S. Vynckier, "Absorbed dose determination in external beam radiotherapy: An international code of practice for dosimetry based on standards of absorbed dose to water," 2004. [Online]. Available: http://www-naweb.iaea.org/nahu/dmrp/pdf_files/CoPV11b.pdf

[25] L. Raffaele, G. A. P. Cirrone, G. Cuttone, S. Lo Nigro, M. G. Sabini, V. Salamone, E. Egger, A. Kacperek, and N. Romeo, "Proton beam dosimetry for the CATANA project," *Phys. Med.*, vol. XVII, no. suppl. 3, pp. 35–40, 2001.

[26] G. A. P. Cirrone, G. Cuttone, F. Di Rosa, S. Lo Nigro, and G. Russo, "Piani di trattamento per protonterapia oculare con metodo Monte Carlo," *Rapporti ISTISAN*, vol. 06/54, pp. 26–34, 2006.